BULLETIN OF THE POLISH ACADEMY OF SCIENCES
TECHNICAL SCIENCES, Vol. 73(5), 2025, Article number: e154720
DOI: 10.24425/bpasts.2025.154720

CIVIL ENGINEERING

Pile-base resistance formation in natural-scale field conditions

Paweł SIEMASZKO *

Unaffiliated

Abstract. Field testing is the most relevant method for verifying pile foundation design calculations. The ultimate static load test allows the pile load to reach the maximum bearing capacity; however, the excessive cost of this method restricts its use. The theory presented in this paper is based on static load test results performed in a specifically designed chamber that closely resembles natural soil conditions and pile dimensions. This study utilizes the Meyer-Kowalow theory and previous author's work on this topic to attain a streamlined design process and reduce costs without compromising safety and reliability. It was concluded that the relationship between the toe and skin of the pile remained constant, and this was depicted in graphs showing the results under field conditions. The author intends to verify this conclusion in future research, using more static load test results. The primary focus of this study was to develop a method for estimating pile-toe bearing capacities, which represents the most complex measurement method to solve. The previous author's works focused on developing the calculus required to estimate the pile-skin bearing capacity, which was the first step in describing the pile-soil interaction. This study focused on verifying a mathematical model describing pile-toe behavior and calculations based on this model. This study provides practical equations for estimating pile-toe and skin resistance, which can improve the design process when using the proposed method.

Keywords: static load test; pile base resistance; load-settlement curve; pile-bearing capacity.

1. INTRODUCTION

This study covered a broad range of practical engineering applications. An essential aspect of a deep foundation is the mechanism of skin-resistance formation, that is, the resistance between the soil and the foundation surface. For example, this occurs in various pile technologies, such as retaining walls, sheet piles, and other underground constructions. Therefore, this study aimed to accurately define the formation of skin resistance between the soil and the foundation. In practical cases, skin resistance can be defined as the difference between the loads at the top and bottom of the foundation. The primary aim was to define the dependence of the bottom resistance and load at the top of the pile. Typically, the static load test method is applied to estimate toe and skin resistance. These test results are often depicted using a Q-s curve, which represents the relationship between the load placed on the head of the pile and the resulting settlement measured as the downward movement of the pile from the level of its initial head position. This curve type was proposed using the Brinch-Hansen 80% [1], Chin-Kondner [2], and Decourt [3] methods. Recently, a new method termed the Meyer-Kowalow (M-K) curve has been included. Examples of this approach are shown in Figs. 1–4.

Comparatively, for the previously proposed methods, the M-K curve [4, 5] satisfies the physical boundary conditions of the Bousinessq description. For a small load value, the dependence between load and resistance is linear. When the settlement is uncontrolled, the critical load value is described using a vertical asymptote. Experimental research was conducted on the M-K model to validate the proposed mechanisms of the formation and skin resistance in pile foundations.

The aforementioned methods were previously developed and serve as a basis for pile-bearing capacity analysis. The Brinch-Hansen 80% method assumes that the ultimate settlement s_u is greater than four times the settlement value at 80% of the ultimate bearing capacity. By drawing a linear dependence between the settlement and load as $\sqrt{s}/Q$ and approximating $\sqrt{s}/Q = A \cdot s + B$, a graph can be created, and the ultimate capacity can be calculated. A sample graph is shown in Fig. 1,

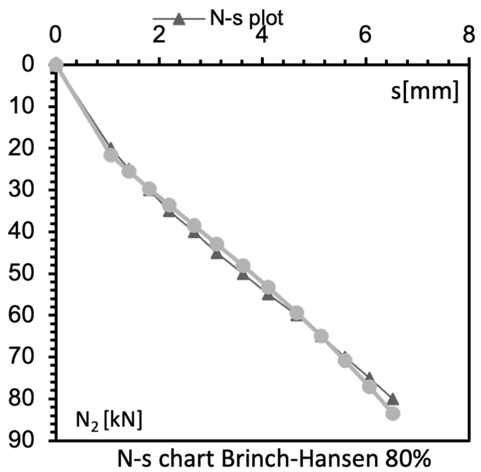

Fig. 1. Brinch–Hansen 80% method N-s graph compared to measured values

*e-mail: pw.siemaszko@gmail.com

Manuscript submitted 2025-01-19, revised 2025-04-02, initially accepted for publication 2025-05-11, published in August 2025.

where $Q = N_2$ – load in the head of the pile, $\sqrt{s}$ – squared root of settlement value, A, B – values of approximated linear relationship between s, Q.

The ultimate capacity Q_u is calculated using the following equation, where A, B – values of an approximated linear relationship between s, Q

$$Q_u = \frac{1}{2\sqrt{A \cdot B}} \text{ [kN]}. \tag{1}$$

The method presented by Chin and Kondner is based on the linear equation $f(s) = s/Q$. By approximation, the relationship can be calculated as $s/Q = A \cdot s + B$, B – values of approximated linear relationship between s, Q. Using this equation, the load-settlement curve is derived in Fig. 2.

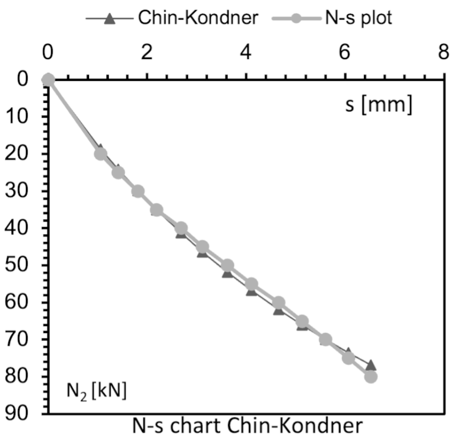

Fig. 2. Chin-Kondner method N-s graph, compared to measured values

The ultimate bearing capacity is calculated using the following equation

$$Q = \frac{1}{A} \text{ [kN]}. \tag{2}$$

The Decourt method uses the function $f(s) = Q/s$, and a linear relationship is obtained using the approximation $Q/s = A \cdot Q + B$. The load-settlement curve was derived based on this function in Fig. 3.

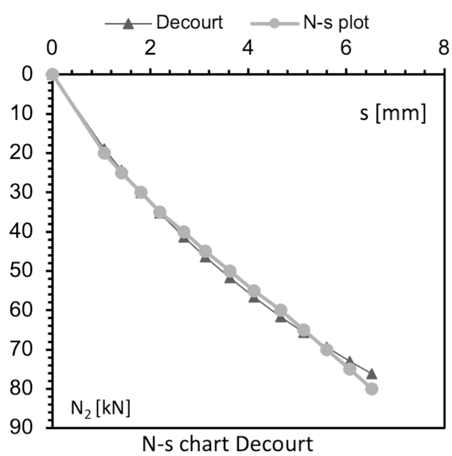

Fig. 3. Decourt method N-s graph compared to measured values

The ultimate bearing capacity is calculated using the following equation

$$Q_u = -\frac{B}{A} \text{ [kN]}. \tag{3}$$

All graphs were constructed using the data presented in Table 1.

Table 1
Static load test data and values calculated using different methods

s [mm]	N [kN]	$N_{\text{Brinch-Hansen}}$	$N_{\text{Chin-Kondner}}$	N_{Decourt}
0	0.00	0	0	0
1.06	20.00	21.66	18.75	18.90
1.41	25.00	25.57	24.17	24.3
1.81	30.00	29.77	29.96	30.0
2.19	35.00	33.62	35.10	35.21
2.68	40.00	38.52	41.27	41.33
3.12	45.00	42.94	46.41	46.41
3.62	50.00	48.07	51.84	51.76
4.11	55.00	53.26	56.78	56.62
4.66	60.00	59.38	61.94	61.67
5.13	65.00	64.90	66.04	65.68
5.6	70.00	70.76	69.89	69.44
6.07	75.00	77.03	73.51	72.96
6.52	80.00	83.47	76.79	76.14

s [mm] – pile settlement measured at the head.
N [kN] – load measured under the pile base using a specific measurement mat.
$N_{\text{Brinch-Hansen}}$ [kN] – pile load calculated using the Brinch-Hansen method.
$N_{\text{Chin-Kondner}}$ [kN] – pile load calculated using the Chin-Kondner method.
N_{Decourt} [kN] – pile load calculated using the Decourt method.

2. MEYER-KOWALOW CURVE AND PILE-BEARING CAPACITY

The M-K method was introduced in 2010 [5] as a solution for drawing a continuous load-settlement curve that represents the boundary-bearing capacity of a pile and is based on the obtained $\{N_i; s_i\}$ values during a static load test. The literature includes many methods for drawing load-settlement curves [6–9] that do not consider the physical aspects of loading. The M-K method was developed using Kirchhoff's principle and the physical assumption that the representative curve has two asymptotes:

1. The loading limit of a pile causing uncontrolled settlement is represented by a vertical asymptote.
2. The diagonal asymptote, which crosses the origin and marks the linear load-settlement relationship for lower loading values, follows Boussinesq's theory.

Kirchhoff's principle and the assumption of two physical asymptotes allow us to consider the pile-soil interaction at full scale with a mathematical description. This approach combines the experience obtained in the field of pile testing with research conducted on this topic. Load-settlement curves were drawn based on the results obtained from testing, and calculations were performed to fit the obtained results. Combining the mathematical model with the pile static load test results represented as a load-settlement curve provides the possibility of designing piles with better geometry optimization and optimal bearing capacity.

Considering these assumptions, the M-K method can be used to draw a curve for the given $\{N_i; s_i\}$ values as input data. The parameters N_{gr}, κ_2, C_2 are obtained through approximation and are used to describe the M-K curve using (4)

$$s = C_2 N_{gr,2} \frac{\left(1 - \frac{N_2}{N_{gr,2}}\right)^{-\kappa_2} - 1}{\kappa_2}, \qquad (4)$$

where
C_2 – reversed aggregated Winklers modulus $\left[\frac{\text{m}}{\text{MN}}\right]$ parameter.
$N_{gr,2}$ – axial force; M-K curve vertical asymptote [MN].
κ_2 – parameters showing the proportions of base and shaft resistances.

An example of an M-K curve is shown in Fig. 4.

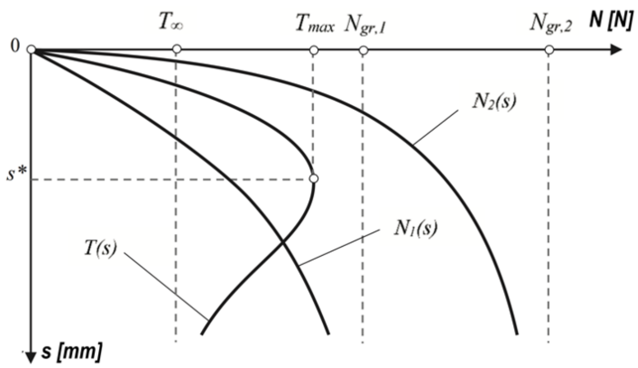

$T(s)$ [kN] – skin resistance of pile graph.
$T_{\max}$ [kN] – boundary value of the pile-skin resistance. After exceeding this value, the soil slips on the surface of the pile, which causes the settlement to rise uncontrollably.
$N_{gr,1}$ [kN] – boundary value of pile-toe resistance.
$N_2(s)$ – pile-bearing capacity.
$N_1(s)$ [kN] – pile-toe bearing capacity.

Fig. 4. M-K curve showing vertical asymptote and differentiation of forces that contribute to the pile-bearing capacity

It can be demonstrated that the Chin-Kondner curve is an M-K curve for $\kappa_2 = 1$ [10, 11]. In practical cases, κ_2 varies from 0 to 2. Previous studies based on static sounding, i.e., CPTu investigations, suggest that the M-K curve parameters can be based on CPTu results with sufficient accuracy. It is possible that if optimization is required to change the geometry and soil in certain cases, the CPTu test is sufficient to estimate the M-K curve parameters. Examples of this estimation, based on soil sounding, are provided in equations (18)–(21). The skin resistance of a pile can be estimated using the M-K theorem [11, 12]. When the skin resistance of a pile is known, the complete solution for a single pile-soil interaction can be described.

Researchers continue to study extensively and discuss the pile-bearing capacity to provide the best viable solutions for engineering design and execution. In recent years, discussions have focused on analyzing past failures [13], CPTu-based estimations of pile capacity [14–17], and improving the relationships formed over many years [18].

Currently, certain approaches appear to be more accurate for field measurements of static load tests, using gauges or fiber-optic sensors as tools for estimating pile-skin resistance [19–21]. This method facilitates the measurement of skin-resistance formation as a function of pile loading and increased settlement, which is crucial for determining a mathematical description of the phenomena. It is important to emphasize that soil profiles vary from country to country and that the local environment must be considered when presenting the results. Many authors acknowledge this fact and have attempted to verify whether the approaches from earlier publications can be updated. For example, the method of estimating pile-skin resistance can be compared by analyzing the CPTu soil investigation results along with the pile-bearing capacity [3, 18, 22]. There are still publications that compare SPT investigation results as a tool for estimating pile-skin resistance based on past approaches [23], using strain gauges to measure axial changes along the pile shaft. The CPTu soil investigation method is most relevant to the pile-skin resistance behavior. Cones pressed into the soil under the load surpassed the static friction between the cone surface and the soil. However, most piles are not loaded to surpass the static friction between the pile surface and soil; therefore, they should not exhibit identical behavior.

For practical engineering calculations, the description of the pile-skin resistance as a change in the axial pile force provides satisfactory results and is included in the description. The pile-skin resistance is the difference between the head load and the resistance of the soil against the pile, which is tangential to the pile skin with the vertical direction pointing toward the head of the pile. Studies on skin resistance, including the M-K curve theorem, were initially conducted using laboratory model cases [11, 24].

Combining the proposed load-settlement curve estimation theory for predicting the ultimate bearing capacity with sufficient static load test results allows for a better understanding of pile behavior, leading to more economical and reliable design outcomes. Despite wide research and numerous comprehensive descriptions presented over the years [25–27], as well as recent papers attempting to describe pile-soil phenomena and improve the design process, there remains a need to enhance the understanding of the processes involved in determining the ultimate bearing capacity of piles [12, 28].

In this study, a field experimental analysis was conducted to verify whether the vertical distribution could be described as a linear relationship between N_2 (load at the head of the pile) and N_1 (skin resistance). This suggests that the resistance of the pile toe is linear in the upward direction toward the head of the pile.

Three static load tests reflecting the natural conditions of the pile were conducted on a full-scale platform at a construction site.

3. FIELD EXPERIMENTS IN NATURAL SCALE

The main purpose of constructing the platform was to create a pile environment that closely resembled the natural conditions. The constructed platform measures 2.2 m in width, 2.4 m in length, and 6.0 m in height. It was built on a 300 cm × 300 cm × 50 cm reinforced concrete foundation, which included a steel beam to facilitate the static load test in accordance with the Polish Code PN-83/B-02482 [29]. The platform is illustrated in Figs. 5 and 6.

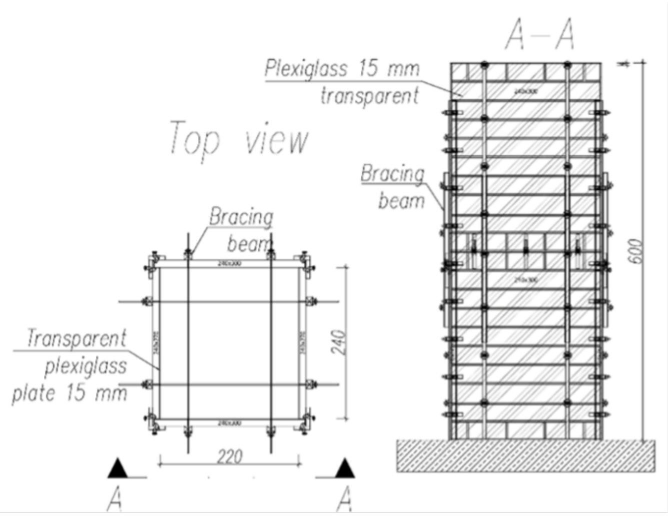

(a)

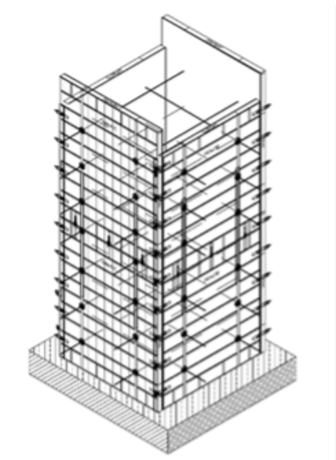

(b)

Fig. 5. Field research stands for pile load testing. Dimensions of the chamber: (a) top view and cross-section; (b) 3D model of the chamber [30]

Inside the constructed chamber, a non-cohesive soil profile was formed with densified layers 10–15 cm in thickness. The piles were installed as displacement piles and were placed on an experimental platform using a crane. Additional layers were added to fill the chamber and complete the experimental field stand. An axial load was applied to the head in stages, with each stage maintained until the settlement value stabilized. For each settlement value, the load at the head, settlement value, and stress under the pile base were measured.

(a) (b)

Fig. 6. Photographs of field research stand for pile load test: (a) transparent chamber filled with soil; (b) pile used in the investigations [30]

To obtain stress values under the pile base, a flexible sensor consisting of polymer layers covering a stress-sensitive semiconductor on both sides was used. The sensor measuring 425 mm × 425 mm with a thickness of 0.381 mm is shown in Fig. 7. The values obtained were precise because the sensor contained 1936 measuring points. The flexibility of the sensor helps avoid the influence of changing soil properties.

Fig. 7. Photograph of the sensor used in the experiment

The sensor enabled measurement of the base resistance within its area, which was subsequently calculated. This value is denoted as N_1. The obtained values are shown in the following graphs in Fig. 8.

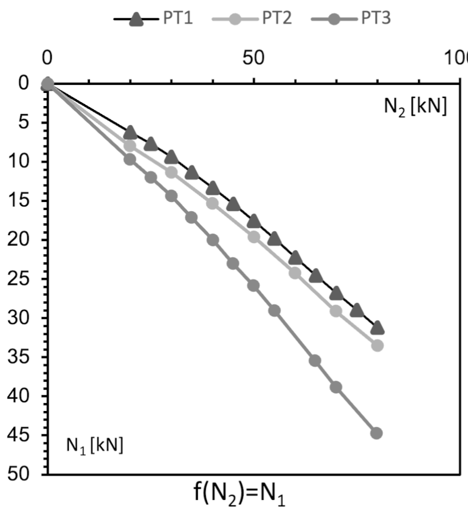

Fig. 8. $N_2\,(N_1)$ relationship of measured values for PT1, PT2, PT3

4. RESULTS OF FIELD EXPERIMENTS

Using the obtained data, the parameters N_{gr}, κ_2, and C_2 were estimated and organized in tables, followed by graphs presenting the relationship between N_2 and (N_1) for piles PT1, PT2, and PT3.

A linear relationship $N_2\ (N_1)$ was observed in the results. To verify this, a mathematical approach was used to analyze the graphs.

5. MATHEMATICAL DESCRIPTION

A set of data $\{N_i; s_i\}$ was provided from the static load test, including both $\{N_2; s_i\}$ and $\{N_1; s_i\}$, where Indices 2 and 1 correspond to the loads measured at the head and base of the pile, respectively.

Analysis of the static load test data demonstrates that the correspondence between the toe resistance and pile-bearing capacity $N_1 = f(N_2)$, as suggested in a previous study [19], appears to be linear for loads $N_2 < 80$ kN

$$N_1 = f(N_2) = a + b \cdot N_2 . \tag{5}$$

To verify whether a linear distribution best fits the obtained results, the least-squares analysis was conducted using four types of distributions:

1. $y = a + bx,$ (6)
2. $y = a \cdot x^b,$ (7)
3. $y = a + b \cdot \ln x,$ (8)
4. $y = a \cdot b^x.$ (9)

For a given set of data $\{N_2; s_i; N_1\}$, the following correlations were obtained from the above graphs:

1. $N_1 = -1.145 + 0.3893 N_2;$ $\quad r = 0.993,$ (10)
2. $N_1 = 0.504 \cdot N_2^{0.9075};$ $\quad r = 0.974,$ (11)
3. $N_1 = -21.08 + 10.5513 \cdot \ln N_2;$ $\quad r = 0.892,$ (12)
4. $N_1 = 3.398 \cdot 1.0308^{N_2};$ $\quad r = 0.985.$ (13)

It is shown that for every type of analyzed graph, a satisfactory correlation was obtained, as measured by the parameter

$$r \in \langle 0; 1 \rangle .$$

From the results presented in the table, it can be concluded that different graphs exhibit a better correlation for different segments of N_2 values. For practical applications, it is essential to verify the correlation for larger values of load $N_1 = f(N_2)$ in a linear form.

From the results presented in the table, it can be concluded that, for practical calculations, the following linear dependence is sufficient when considering the load at the head and toe resistance

$$N_1 = -1.145 + 0.3893 N_2 . \tag{14}$$

The graphs of the values obtained during the experiment are compared with the calculated values in Figs. 9–11.

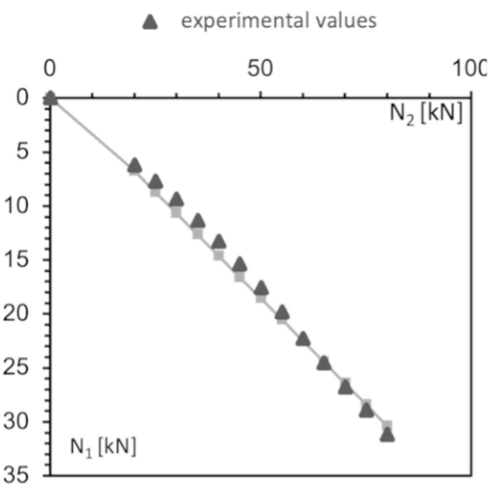

Fig. 9. Linear approximation compared to PT1 experimental values

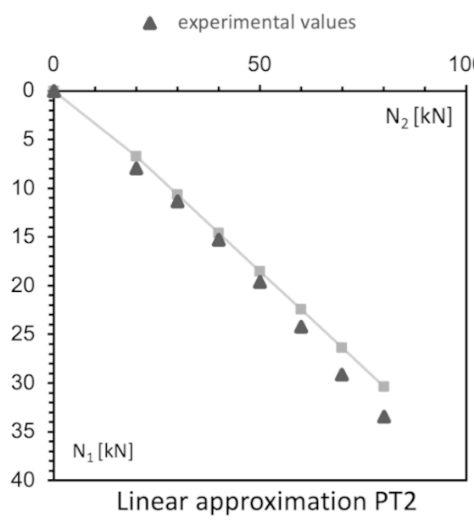

Fig. 10. Linear approximation compared to PT2 experimental values

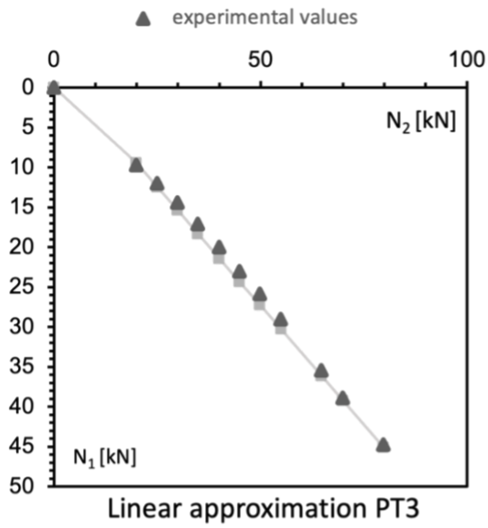

Fig. 11. Linear approximation compared to PT3 experimental values

However, a more detailed analysis revealed that the relationship between the load at the head and toe resistance was a function of κ_2. To further consider the relationship between N_1 (N_2), we proceed with (15).

The next step is to analyze the relationship $N_1 = f(N_2)$ using the following equation

$$N_1 = \frac{N_2}{(1+\kappa_2)^n}. \tag{15}$$

Using linear equation (12), the following correlation is possible

$$(1+\kappa_2)^n = \frac{N_2}{-1.145+0.3893\cdot N_2}. \tag{16}$$

This allows us to present the value of n as

$$n = \frac{\ln\left(\dfrac{N_2}{-1.145+0.3893\cdot N_2}\right)}{\ln(1+\kappa_2)}. \tag{17}$$

The value of n calculated using (17) depends on the values of N_2 and κ_2.

Based on Table 2, for larger N_2 values $\left(N_2 > \frac{1}{2}N_{2\max}\right)$, which are the most meaningful values for practical calculations, the value of n' may be presented as $n = n(\kappa_2)$, as shown in Table 3.

The values presented in the table can be expressed as nonlinear relationships. The best correlation was obtained using (18)

$$n = n(\kappa_2) = 1.51\cdot\left(\frac{1}{\kappa_2}\right)^{1,5}, \tag{18}$$

where the correlation coefficient $r = 0.993$.

This allowed us to estimate an equation that best fits the curve from Table 2, expressed as (15) where it is assumed that $\kappa_2 > 0.2$.

According to a previous study [31], M-K curve parameters can be obtained from (19)–(21) if the $q_c(z)$ values from the CPTu investigation are available. For practical calculations, the following was used

$$C_1 = \frac{1}{\pi D q_b\cdot(1+\kappa_2)^{\frac{3}{4}}\cdot\left(1+\frac{1}{4}q_b^{\frac{1}{3}}\right)}, \tag{19}$$

Table 2
Values of n calculated using (17)

N_2 [kN]	κ_2 [–]							
	0.2	0.4	0.6	0.8	1.0	1.5	2.0	3.0
5.00	10.04	5.44	3.89	3.11	2.64	2.00	1.66	1.30
10.00	7.08	3.83	2.74	2.20	1.86	1.41	1.17	0.93
15.00	6.37	3.45	2.47	2.00	1.67	1.26	1.05	0.83
20.00	6.04	3.27	2.34	1.80	1.59	1.20	1.00	0.79
25.00	5.86	3.17	2.27	1.81	1.54	1.16	0.97	0.77
30.00	5.74	3.11	2.22	1.78	1.51	1.14	0.95	0.75
35.00	5.65	3.06	2.20	1.75	1.48	1.12	0.93	0.74
40.00	5.59	3.03	2.17	1.73	1.47	1.13	0.92	0.73
45.00	5.54	3.00	2.15	1.72	1.46	1.10	0.92	0.73
50.00	5.50	2.98	2.13	1.70	1.44	1.10	0.91	0.72
55.00	5.47	2.96	2.12	1.69	1.44	1.10	0.91	0.72
60.00	5.45	2.95	2.11	1.69	1.43	1.08	0.90	0.71
65.00	5.42	2.94	2.10	1.68	1.42	1.08	0.90	0.71
70.00	5.40	2.93	2.09	1.67	1.42	1.07	0.89	0.71
75.00	5.39	2.92	2.09	1.67	1.41	1.07	0.89	0.71
80.00	5.38	2.91	2.09	1.66	1.41	1.07	0.89	0.71

Table 3
κ_2 values for larger head loads $N_2 > 0.5N_{2\max}$ shown in Fig. 12

κ_2	0.20	0.40	0.60	0.80	1.00	1.50	2.00	3.00
ref. n	5.50	3.00	2.00	1.75	1.50	1.10	0.90	0.70

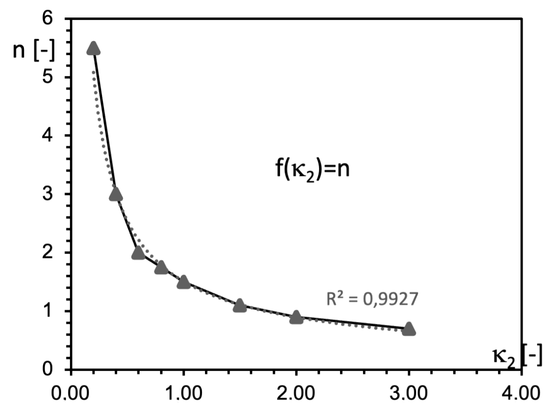

Fig. 12. Graph showing n and κ_2 dependencies as in Table 3

$$N_{gr1} = \frac{1}{2\pi} \cdot q_b \cdot D^2 \cdot \left(\frac{h}{D}\right)^{\frac{1}{3}}, \tag{20}$$

where q_b denotes the static-sounding CPTu and q_c test cone resistance at the toe depth of the pile.

Examples of the results obtained using this calculation method for the static load tests are shown in Figs. 13–15.

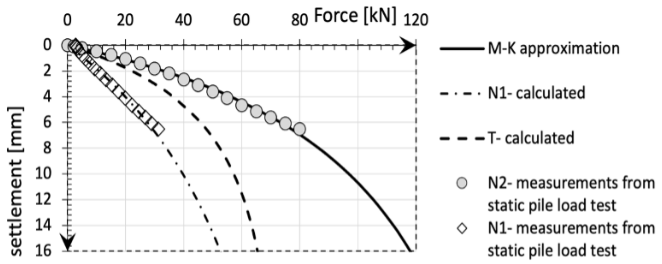

Fig. 13. Graph presenting the distribution of components of pile resistance and M-K curve approximation for PT1 [30]

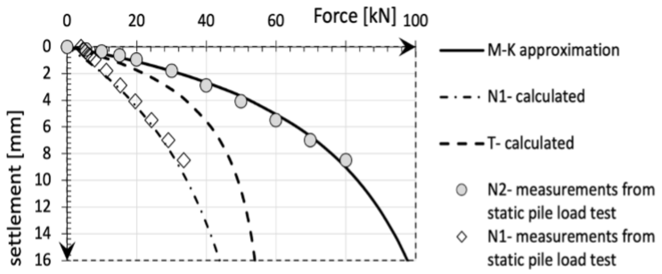

Fig. 14. Graph presenting the distribution of components of pile resistance and M-K curve approximation for PT2 [30]

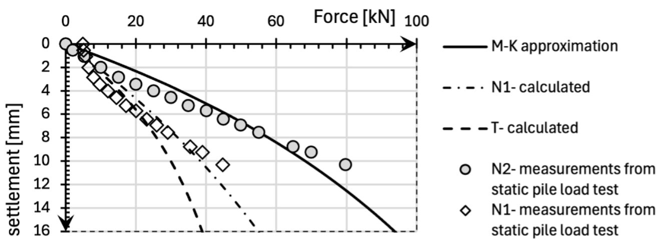

Fig. 15. Graph presenting the distribution of components of pile resistance and M–K curve approximation for PT3

Based on the obtained results, the following equation was formulated, which included the M-K theory assumptions and static load test results

$$C_2 = \frac{C_1}{(1+\kappa_2)^n}. \tag{21}$$

6. CONCLUSIONS

1. This paper presents the experimental results of pile-based resistance in chambers offering close resemblance to natural soil conditions. These results verified the mechanism of toe-resistance formation during static load testing. During these tests, a measuring unit with 1936 measurement points was spread consistently across the pile base surface, facilitating the total toe resistance and distribution of the vertical component of the resistance to be obtained.
2. The experiments demonstrated that, for practical engineering calculation purposes, the base resistance of the pile is a constant value relative to the skin resistance during the loading procedure. The obtained results allowed for the formulation of equations that enabled the determination of this ratio. From the obtained results, it was observed that the agreement between the measured and calculated static load test results was sufficient for practical engineering calculations.
3. Equations (18)–(21) allow us to obtain M-K parameters based on the sounding soil using CPTu technology. This provides a tool for the initial estimation of pile-bearing capacity using the soil profile during the early design process.
4. For the field experiments presented in this paper, it was observed that the toe resistance is a fraction of the head load and that this fraction does not change with settlement during the static load test. This is an important finding because it makes the full solution to the pile-resistance problem more practical.
5. The M-K curve equation includes the ratio between the load at the head of the pile N_2, and the boundary-bearing capacity of pile N_{gr}. N_{gr} denotes the value of the load that causes the settlement of the pile to increase out of control. The ratio N_2/N_{gr} may be considered a safety factor, which could be used to improve the design process and the application of soil mechanics to the pile-bearing capacity.
6. The proposed approximation method for M-K curve parameters facilitates a more precise estimation of the skin resistance when the settlement is changed. This method facilitates the safe design of piles while incorporating proper soil-pile mechanics.
7. Improvements in measurement tools have led to a better description of pile-soil interactions. The evolution of the M-K method may lead to a complete mathematical description of pile-soil interactions. Future research will aim to conduct more static load tests equipped with strain gauges or fiber-optic sensors to gather skin-resistance data using various technologies.

REFERENCES

[1] J.B. Hansen, "Discussion of "hyperbolic stress-strain response: Cohesive soils," *J. Soil Mech. Found. Div.*, vol. 89, no. 4, pp. 241–242, 1963, doi: 10.1061/JSFEAQ.0000542.

[2] F.K. Chin, "Estimation of ultimate load of piles not carried to failure," in Proc. 2^{nd} *Southeast Asia Conference on Soil Engineering*, 1970, pp. 81–92.

[3] L. Decourt, "Behaviour of foundations under working load conditions," in Proc. of the 11^{th} *Pan-American Conf. on Soil Mechanics and Geotechnical Engineering*, Dolgassau, Brasil, 1999, vol. 4, pp. 453–488.

[4] A. Góral, "Direct and Inverse Artificial Neural Networks as Auxiliary Tools in Numerical Solutions of Selected Problems of Soil-

Structure Interaction in Geotechnical Engineering," Doctoral dissertation, Łódź University of Technology, Poland, 2023.

[5] Z. Meyer, "Analysis of stresses on the side and base of a single pile based on the linear Boussinesq theory," presented at the *XVIII Scientific Seminar, Regional Environmental Engineering Problems*, West Pomeranian University of Technology, Szczecin, 2010.

[6] J.-L. Briaud. *Geotechnical Engineering: Unsaturated and Saturated Soils*. Chichester, England: John Wiley & Sons, 2013, doi: 10.1002/9781118686195.

[7] K. Duffy, K. Gavin, M. Korff, and D. de Lange, "Base resistance of screw displacement piles in sand," *J. Geotech. Geoenvironm. Eng.*, vol. 150, no. 8, 2024, doi: 10.1061/JGGEFK.GTENG-12340.

[8] H.G. Poulos and E.H. Davis. *Pile Foundation Analysis and Design*. New York: John Wiley & Sons, 1980.

[9] H.S. Thilakasiri, "Qualitative interpretation of load-settlement curves of bored piles," *Eng. J. Inst. Eng. Sri Lanka*, vol. 40, no. 4, p. 61, 2007, doi: 10.4038/engineer.v40i4.7155.

[10] G. Szmechel, "Determination of the ultimate bearing capacity of piles based on static load tests in a limited range," Doctoral dissertation, West Pomeranian University of Technology, Szczecin, 2014.

[11] K. Żarkiewicz, "Analysis of the formation of side resistance of a pile in non-cohesive soils based on model laboratory tests," Doctoral dissertation, West Pomeranian University of Technology, Szczecin, 2017.

[12] P. Siemaszko and Z. Meyer, "Analysis of the pile skin resistance formation," *Stud. Geotech. Mech.*, vol. 43, no. 4, pp. 380–388, 2021, doi: 10.2478/sgem-2021-0026.

[13] G.B. Baecher, "2021 Terzaghi lecture: Geotechnical systems, uncertainty, and risk," *J. Geotech. Geoenvironm. Eng.*, vol. 149, no. 3, p. 03023001, 2023, doi: 10.1061/JGGEFK.GTENG-10201.

[14] M. Karimpour-Fard and A. Eslami. "Estimation of vertical bearing capacity of piles using the results CPT and SPT tests," in *Geotechnical and Geophysical Site Characterization*, Taylor & Francis Group, 2013, pp. 1055–1062.

[15] A. Krasiński and M. Wiszniewski, "Static load test on instrumented pile – field data and numerical simulations," *Stud. Geotech. Mech.*, vol. 39, no. 3, pp. 17–25, 2017, doi: 10.1515/sgem-2017-0026.

[16] M. Stęczniewski, "Assessment of pile bearing capacity based on CPT probe tests," Doctoral dissertation, Gdańsk University of Technology, 2003.

[17] P. Więcławski, "Prediction of the performance of axially loaded Vibro piles using CPT probing results," Doctoral dissertation, Gdańsk University of Technology, 2016.

[18] E.M. Comodromos and M.F. Randolph, "Improved relationships for the pile base response in sandy soils," *J. Geotech. Geoenvironm. Eng.*, vol. 149, no. 8, 2023, doi: 10.1061/JGGEFK.GTENG-11035.

[19] B. Fellenius and T. Ruban, "Analysis of strain-Gage records from a static loading test on a CFA pile," *DFI J.-J. Deep Found. Inst.*, vol. 14, no. 1, pp. 39–44, 2020, doi: 10.37308/DFI-Jnl.20181008.189.

[20] J.K. Kania, K.K. Sørensen, and B.H. Fellenius. "Driven piles installed in soft soils subjected to vertical and lateral soil movement," presented at the *Canadian Geotechnical Society, Annual Geotechnical Conference, Geovirtual2020*, Calgary, Canada, 2020.

[21] J.K. Kania, K.K. Sørensen, and B.H. Fellenius, "The development of units shaft resistance along driven piles in subsiding soil," *Can. Geotech. J.*, vol. 61, no. 5, pp. 1035–1050, 2024, doi: 10.1139/cgj-2022-0694.

[22] B.M. Lehane *et al.*, "CPT-based axial capacity design method for driven piles in clay," *J. Geotech. Geoenvironm. Eng.*, vol. 148, no. 9, p. 04022069, 2022, doi: 10.1061/(ASCE)GT.1943-5606.0002847.

[23] Y. Coriat and S. Frydman, "Estimation of shaft and base resistances of cast-in-place piles in Israel from analysis of pile loading tests," *J. Geotech. Geoenvironm. Eng.*, vol. 149, no. 4, p. 04023009, 2023, doi: 10.1061/JGGEFK.GTENG-10997.

[24] Z. Meyer, "Use of static pile test results to determine the mobilization of side resistance," presented at the *Regional Environmental Engineering Problems Conference*, West Pomeranian University of Technology, 2015.

[25] J. Knappett and R.F. Craig, *Craig's soil mechanics*, 8th ed., Boca Raton, FL: CRC Press, 2011.

[26] D. Tara and S. Coulter. "Interpretation of static pile loading test results and application for design of pile groups." Vancouver Geotechnical Society. 2015. [Online]. Available: https://static1.squarespace.com/static/523c951be4b0728273e73d94/t/55889325e4b0a99e3064a611/1435013925102/Paper+4+-+Tara.pdf. [Accessed: 29 Dec. 2024].

[27] M.J. Tomlinson and J. Woodward, *Pile design and construction practice*, 5th ed. Boca Raton, FL: CRC Press, 2007.

[28] P. Siemaszko, "Pile–Soil Interaction during Static Load Test," *Stud. Geotech. Mech.*, vol. 46, no. 3, pp. 164–175, 2024, doi: 10.2478/sgem-2024-0010.

[29] Polish Committee for Standardization, "PN-83/B-02482: Bearing capacity of piles and pile foundations," Polish Standard, 1983.

[30] Z. Meyer, P. Siemaszko, and K. Zarkiewicz, "Experimental research of pile toe resistance in natural conditions," *Arch. Civ. Eng.*, vol. 70, no. 3, pp. 313–323, 2024, doi: 10.24425/ace.2024.150985.

[31] P. Siemaszko and Z. Meyer, "Static load test curve analysis based on soil field investigations," *Bull. Pol. Acad. Sci. Tech. Sci.*, vol. 67, no. 2, 2019, doi: 10.24425/bpas.2019.128607.